Open Access Article

Tension-Resisted Steel Base Isolation for Reducing Seismic Responses on Steel Frame Models Using Time History Analysis and One-Direction Shaking Table Test Considering the Different Amounts of Sliding Roller Rods

Taufiq Rochman[1*], Evi Nur Cahya[2], Eva Arifi[3], Ahmad Kahfi Firdausi[4]

[1] Civil Engineering Department, State Polytechnic of Malang, Malang, Indonesia

[2] Water Resources Engineering Department, Brawijaya University, Malang, Indonesia

[3] Civil Engineering Department, Brawijaya University, Malang, Indonesia

[4] Master Student of Construction Management, Civil Engineering Department, Brawijaya University, Malang, Indonesia

Abstract: Although much research has been focused on seismic isolation, there is very limited research on steel-made base isolation to minimize structural building damage. The purpose of this research is to design a new steel base isolation instead of three previous models that are lead rubber bearing (LRB), high damping rubber bearing (HDRB), friction pendulum system (FPS). A new tensile-resisted base isolation system support model that also utilized inserted sliding roller rods to improve earthquake resistance has been proposed. These new models also utilize the returning curvature scheme to deliver roller rods into their original positions. The steel frame models of 5, 10, and 15 storeys will be used as structures under seismic load to examine the model response. The 1940 El Centro earthquake time history data also verified their performance using 1, 2, and 3 sliding roller rods. Software analysis and shaking table testing were performed to analyze and test under the real vibration. An android-based accelerometer is used to measure the ground floor base motion and steel frame model roof acceleration. The optimum reduction was achieved by three sliding roller rods and likely tends to be better with a larger amount of sliding roller rods' utilization in further research. The optimum seismic responses were significantly reduced by this new steel base isolation system that only works with low-level steel-frame models.

Keywords: tension-resisted steel base isolation, shaking table, time history, steel frame model, sliding roller rods.

使用时程分析和单向振动台试验来减少钢框架模型地震响应的抗拉钢基础隔震考虑不同数量的滑动滚子杆

摘要: 虽然很多研究都集中在隔震上，但对钢制基础隔震的研究非常有限，以最大限度地减少结构性建筑物的损坏。本研究的目的是设计一种新的钢底座隔振器，而不是以前的铅橡胶支座（LRB）、高阻尼橡胶支座（HDRB）、摩擦摆系统（第一人称射击）三种型号。提出了一种新的抗拉基础隔震系统支撑模型，该模型还利用插入的滑动滚子杆来提高抗震能力。这些新型号还利用返回曲率方案将滚子杆传送到其原始位置。5、10、15层钢框架模型将作为地震荷载作用下的结构来检验模型的响应。1940年埃尔森特罗地震时程数据还使用1、2和3个滑动滚柱验证了它们的性能。通过软件分析和振动台试验，在真实振动下进行分析和测试。基于机器人的加速度计用于测量底层基础运动和钢框架模型屋顶加速度。通过三个滑动

Received: June 5, 2021 / Revised: August 8, 2021 / Accepted: September 13, 2021 / Published: October 30, 2021

About the authors: Taufiq Rochman, Civil Engineering Department, State Polytechnic of Malang, Malang, Indonesia; Evi Nur Cahya, Water Resources Engineering Department, Brawijaya University, Malang, Indonesia; Eva Arifi, Civil Engineering Department, Brawijaya University, Malang, Indonesia; Ahmad Kahfi Firdausi, Master Student of Construction Management, Civil Engineering Department, Brawijaya University, Malang, Indonesia

Corresponding author Taufiq Rochman, taufiq.rochman@polinema.ac.id

滚子杆实现了最佳减少，并且在进一步的研究中可能会随着更多的滑动滚子杆的利用而变得更好。这种仅适用于低水平钢框架模型的新型钢基础隔震系统显着降低了最佳地震响应。

关键词：抗拉钢底座隔离、振动台, 时间历史, 钢架模型, 滑动滚轮杆。

1. Background

Earthquake is one of the natural disasters due to the movement of the earth's plates [1]. Advances in research and technology have improved the quality and availability of active fault information and made it possible to understand seismic fault activity better [2].

An earthquake's impact is quite diverse. Earthquake magnitude is an effective proxy for representing seismic hazard intensity and has been used in earthquake disaster damage models [3]. As a result of the damage to these buildings, earthquake force is one of the most important factors in designing a building, especially multi-storey buildings. Together with partitions and the roof, all factors have to be tied collectively to act as an included unit for the duration of earthquake shaking, shifting forces across connections, and stopping separation [4].

In recent years, isolation, energy dissipation, and control systems have been increasingly widely used. Base isolation as a popular and powerful technology can drastically reduce the seismic response of the structure and prevent the structure from damage [5]. Currently, there are nearly 6,500 structures with isolation and about 3,000 structures with passive energy dissipation or hybrid control in China [6].

2. Materials

2.1. Base Isolation Systems

2.1.1. Elastomeric Rubber Bearing

It is a high-strength rubber cushion installed between the foundation and building. This system works by keeping the structure above it as a unit. When an earthquake occurs, each building structure will vibrate due to the ground movement, which affects the building foundation. Because the ground movement is random, the vibrations that enter the structure are also not aligned; this causes a rigid building to collapse easily. In buildings with a base isolator, the vibrations that occur in the foundation will pass through the rubber pads first before entering the structural system. Because the rubber is elastic, the direction of vibration that occurs randomly will only affect the base isolator, while the structure above it will vibrate or move as a single structure [7].

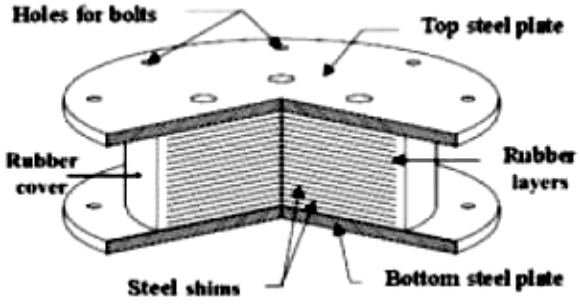

Fig. 1 Base isolator elastomeric rubber bearing [8]

Many experiments concerning seismic reduction systems have been conducted to find the ideal isolation design [9–15]. An experimental study on the effectiveness of a prototype seismic isolation system made from polymeric bearings was performed by Falborski and Jankowski [9]. They stated that the application of the prototype polymeric bearings led to significant improvement in seismic response by reducing the lateral acceleration. Other researchers [5] also statistically investigated the dynamic response of the Nuclear Island building with and without isolators under a typical safe-shutdown earthquake. They found that the results highlighted the drastic reduction of considered floor accelerations as the base isolation major effect [5]. An advanced numerical model of elastomeric seismic isolation bearings was also conducted [10]. The researchers presented the mathematical models of the bearings for the analysis of base isolated structures for design and beyond design basis shaking.

An additional seismic response study [11] concerned the sliding equipment and contents in base-isolated buildings subjected to broadband ground motions. The authors found base isolation to be generally effective in reducing seismic demands on sliding, although, for low friction coefficients and high earthquake intensities, it also increased demands.

Another model was proposed using a magnetorheological elastomer base isolator, in which a second order sliding mode controller was designed and applied to the device to provide real-time feedback control of smart structures [12].

Many analyses and discussions regarding the base isolation system were examined by several researchers [13–17], while a combination of base isolation and tuned liquid column damper and magnetorheological damper was researched in two other studies [18–19].

2.1.2. Friction Pendulum System

A friction pendulum system works like a simple harmonic pendulum with recentering capabilities. One of the main advantages of the friction pendulum system is its ability to return the structure to its original position after the earthquake ends, due to the articulated slider that moves on a concave-shaped stainless-steel surface with a specific curvature value. With the presence of friction resistance on both surfaces, the structure above the basic isolation system will still behave like a fixed-base structure under light lateral load conditions [20].

Additional research has been conducted on the friction pendulum system [21–23]. For instance, one study concerned the restoring capability of friction pendulum seismic isolation systems [21]. Regression analysis was performed to derive the dependency of the residual displacement from the parameters governing the dynamic response of FPS. Other researchers [22] considered different soil conditions to optimally design the friction pendulum system properties for isolated structures. They obtained multi-variate regression expressions for the optimum values of the friction coefficient to minimize the superstructure displacements.

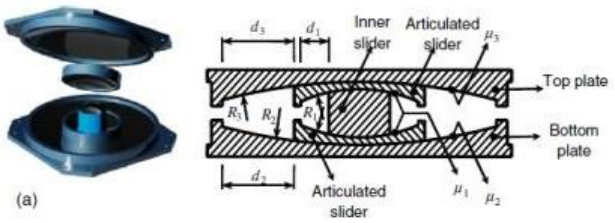

Fig. 2 Triple friction pendulum bearing components [23]

Several shaking table tests also have been conducted [24] regarding the restoring capability of double concave friction pendulum seismic isolation systems. Three different conditions of sliding surfaces corresponding to low, medium and high friction were considered.

2.2. Mechanical Properties of the Friction Pendulum System

The natural period (T) of the friction pendulum bearing is selected simply by choosing the radius of curvature of the concave surface (R) by [25] as

$$T = 2.\pi.\sqrt{\frac{R}{g}} \quad (1)$$

where g is the gravitational acceleration. It is independent of the mass of the supported structure. The lateral stiffness (K) of the bearing provides the restoring capability of the system.

$$K_b = \frac{W}{R} \quad (2)$$

where W is the weight of the structure. As a result, the torsional motions of the structure are minimized since the stiffness center of the bearings coincides with the center of mass of the supported structure.

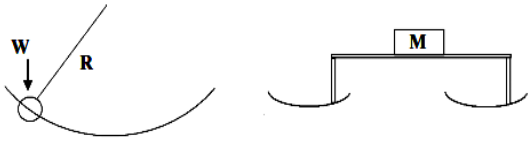

Fig. 3 Concept of sliding pendulum motion [24]

The movement of the slider generates a dynamic friction force that provides the required damping for absorbing the energy of the earthquake. The lateral loads (i.e., the base shear), V, transmitted to the structure as the bearing slides to a distance, u, away from the neutral position include the restoring forces and the friction forces as

$$V = \left(\frac{u}{R} + \mu\right) W \quad (3)$$

where μ is the coefficient of friction. Typical hysteretic loops of the lateral force of FPS in cyclic motion are shown in Fig. 4. The energy (E_D) dissipated for one cycle of sliding with amplitude D is [25] estimated as

$$E_D = 4\mu WD \quad (4)$$

The coefficient of friction depends on the contact pressure between the Teflon-coated slider and the stainless steel surface. The coefficient decreases as the pressure increases. For the FPS to be effective, it is thought that the value of μ should lie between 3% and 10% [25].

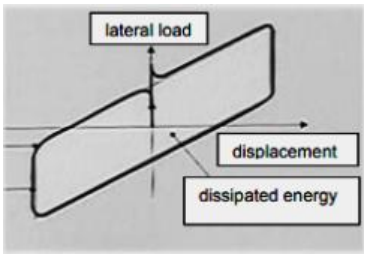

Fig. 4 Hysteresis of lateral load [25]

A brief explanation of this concept also appears in [26]. Research most similar to the steel rolling isolation proposed here was presented in [27], which also reviewed the historical development of and possible future directions for rolling-type seismic isolation.

A previous experimental study [28] used a steel frame and base isolation modeling form by reworking the sliding one-roller concept proposed in [27]; sliding rollers were connected between the foundation and the column as rods. However, previous works still suffer from a disadvantage, namely tensile pull-out force. Hence, it is necessary to improve isolation so as to slightly reduce earthquake energy using the tensile resistance offered by different numbers of inserted sliding roller rods.

2.3. Structural Loading Analysis

2.3.1. Dynamic Analysis

Typically, investigations evaluating the seismic response of base-isolated structures are conducted as follows:

a) Dynamic analysis using a response spectrum: This analysis is conducted under the assumption that the requirements of the code are addressed such that the isolation system can be modeled in terms of equivalent linear elastic behavior.

b) Nonlinear dynamic analysis: A dynamic analysis is performed using seismic time–history accelerograms as the input. It is assumed that the adopted recorded accelerograms are compatible with the reference elastic response spectrum according to the code [29].

Nonlinear dynamic analysis considering damper failure is performed to evaluate seismic responses of steel frames. Moreover, incremental dynamic analysis is employed to ascertain seismic fragility [30].

2.3.2. Static Equivalent Analysis

In the equivalent static force method, the magnitudes of the horizontal loads are computed based on the (first) natural period of the structure. In design practice, the natural period is most commonly determined using the Rayleigh method [31].

2.4. Earthquake Intensity

An earthquake is a physical phenomenon characterized by the shaking of the earth with various intensities [32]. Table 1 shows the intensity of the earthquake as sourced from Indonesian seismic data.

Table 1 Earthquake intensity scale of BMKG [32]

BKG EI Scale	Color	Simple Description	Detailed Description	MMI Scale	PGA (m/s²)
I	White	NOT FELT	Not felt or felt by only a few people but recorded by the tool.	I-II	< 0,029
II	Green	FELT	Felt by the crowd but caused no damage. The light objects that were hanging shook and the glass windows shook.	III-V	0,029 – 0,88
III	Yellow	SLIGHT DAMAGE	The non-structural part of the building suffered minor damage, such as hair cracks on the walls, roof tiles were sliding down and some fell.	VI	0,89 – 1,67
IV	Orange	MODERATE DAMAGE	Many cracks occurred in the walls of simple buildings, some collapsed, broken glass. Part of the plaster of the wall came off. Most of the tiles slide down or fall. The building structure suffered minor to moderate damage.	VII-VIII	1,68 – 5,64
V	Red	HEAVY DAMAGE	Most of the permanent building walls collapsed. The building structure suffered heavy damage. Curved railroad tracks.	IX-XII	> 5,64

2.5. Degree of Freedom

In structural dynamics, the number of independent coordinates necessary to specify the configuration or position of a system at any time is referred to as the number of degrees of freedom. In general, a continuous structure has an infinite number of degrees of freedom. Nevertheless, the process of idealization or selection of an appropriate mathematical model permits the reduction to a discrete number of degrees of freedom. There are some examples of structures that may be represented for dynamic analysis as one-degree-of-freedom systems; that is, these structures are modeled as systems with a single displacement coordinate [33].

2.6. MDOF Forced Vibration Equations

According to Paz and Kim [33], the following equations of motion for a three-storey shear building are obtained by equating the sum of the forces acting on each mass to zero. Hence,

$$m_1\ddot{v}_1 + k_1u_1 - k_2(u_2 - u_1) - F_1(t) = 0 \quad (5)$$

$$m_2\ddot{v}_2 + k2(u_2 - u_1) - k_3(u_3 - u_2) - F_2(t) = 0 \quad (6)$$

$$m_3\ddot{v}_3 + k_3(u_3 - u_2) - F_3(t) = 0 \quad (7)$$

This system of equations constitutes the stiffness formulation of the equations of motion for a three-storey shear building. It may be written conveniently in matrix notation as

$$[M]\{\ddot{v}\} + [K]\{u\} = \{F\} \quad (8)$$

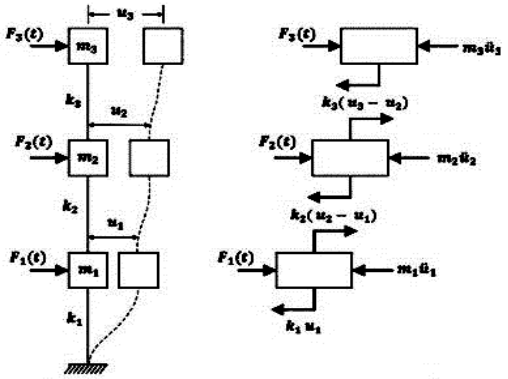

Fig. 5 Modeling as a single column with three DOFs [33]

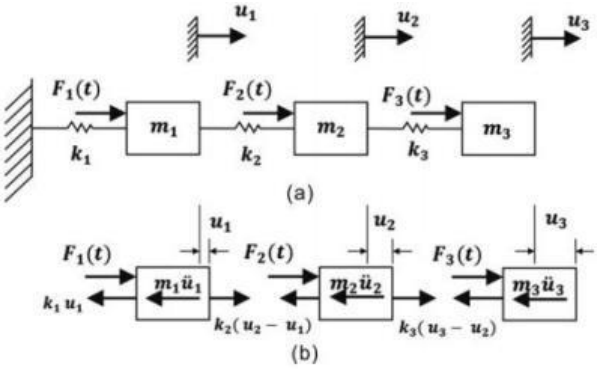

Fig. 6 (a) Multimass-spring model representation of a shear; (b) free body diagram [33]

2.6.1. MDOF Free Vibration Equations

The problem of free vibration requires that the force vector {F} be equal to zero [33], namely,

$$M\{\ddot{u}\} + K\{u\} = 0 \quad (9)$$

The free vibrations of an undamped structure are expressed as the solution of Eq. (10), namely in the form vector notation seen below.

$$\{u_i\} = \{a_i\}\sin(\omega t - a) \quad (10)$$

where a_i is the amplitude of motion of the *i*th coordinate, and n is the number of degrees of freedom. The substitution of Eq. (10) into Eq. (9) gives

$$-\omega^2[M]\{a_i\}\sin(\omega t - a) + [K]\{a_i\}\sin(\omega t - a) = 0 \quad (11)$$

By factoring out $\sin(\omega t - a)$ and rearranging the terms, we see that

$$[[K] - \omega^2[M]]\{a\} = \{0\} \quad (12)$$

Eq. (12) is an eigenproblem. It is a nontrivial solution and requires the determinant of the matrix factor of $\{a\}$ to be equal to zero; hence,

$$|[K] - \omega^2[M]| = 0 \quad (13)$$

2.6.2. MDOF Seismic Excitation Equations

a. Synchronous Ground Motion

The equation of motion of the system depicted here can be formulated by means of the d'Alembert principle; thus, F + T = 0 is applied to each mass [34].

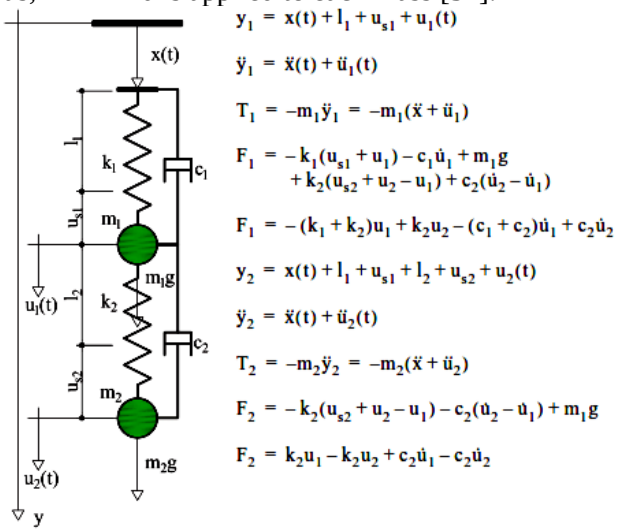

Fig. 7 Equations of motion of the system from the d'Alembert principle [34]

The system of equations governing the motion of the system is expressed as

$$F_1 + T_1 = 0 \quad (14)$$

$$F_2 + T_2 = 0 \quad (15)$$

$$-m_1(\ddot{x} + \ddot{u}_1) - (c_1 + c_2)\dot{u}_1 + c_2\dot{u}_2 - (k_1 + k_2)u_1 + k_2u_2 \quad (16)$$

$$-m_2(\ddot{x} + \ddot{u}_2) + c_2\dot{u}_1 - c_2\dot{u}_2 + k_2u_1 - k_2u_2 \quad (17)$$

The equation of motion of a system subjected to a base excitation is written as

$$M\ddot{u}_a + C\dot{u} + Ku = 0 \quad (18)$$

where $\ddot{u}_a$ is vector of the absolute accelerations of the DOFs of the system, while $\dot{u}$ and u are the vectors of the relative velocities and relative displacements of the DOFs of the system, respectively.

$$u_a = u_s + u \quad (19)$$

where u_s denotes the displacements of the DOFs due to the static application (i.e., it is negligible so that no inertia and damping forces are generated) of the ground motion, and once again, u is the vector of the relative displacements of the DoFs of the system.

The "static displacements" $u_s(t)$ can now be expressed as a function of the ground displacements $u_g(t)$ as follows:

$$u_s(t) = \iota u_g(t) \quad (20)$$

Eq. (18) can now be rewritten as

$$M(\iota\ddot{u}_g + \ddot{u}) + C\dot{u} + Ku = 0 \quad (21)$$

$$M\ddot{u} + C\dot{u} + Ku = -M\iota\ddot{u}_g(t) \quad (22)$$

b. Influence Vector (System with Translation Motion)

In this case, all the DoFs of the system undergo static displacements $u_s(t)$, which are equal to the ground displacement $u_g(t)$ [34]; hence,

$$\iota = \begin{bmatrix} 1 \\ 1 \\ \dots \\ 1 \end{bmatrix} = 1 \quad (23)$$

where 1 is a vector of order (i.e., the number of DoFs) with all elements equal to 1.

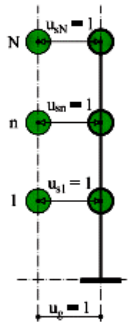

Fig. 8 Planar system with translational ground motion [34]

3. Method

The steel frame models will be tested numerically based on the time–history data of the 1940 El Centro earthquake, with a peak ground acceleration (PGA) of 3.47 m/s^2, as depicted in Fig. 9.

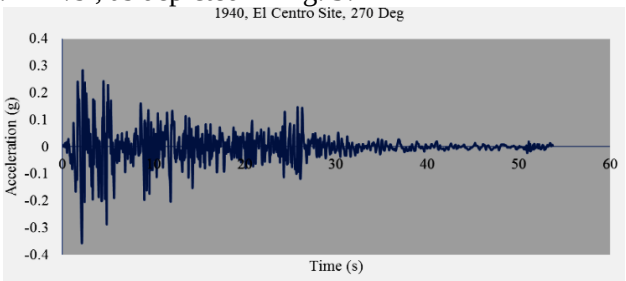

Fig. 9 1940's El-Centro earthquake time history graph

The steel frame models will be analyzed as beam and plate elements, with 5, 10, and 15 storeys representing low-, moderate-, and high-rise buildings, respectively, as depicted in Fig. 10.

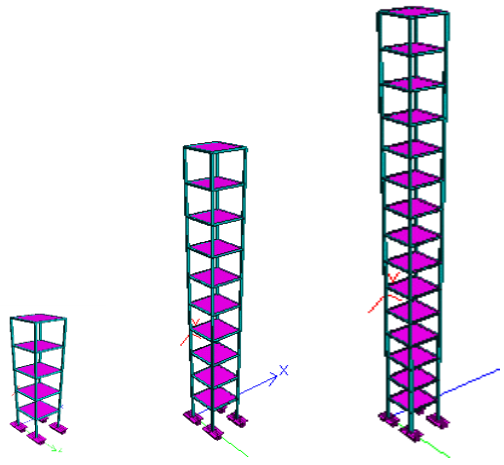

(a) (b) (c)

Fig. 10 Three steel frame STAADPro model prototype for (a) 5 storeys; (b) 10 storeys; (c) 15 storeys

3.1. Multi-Storey Building Steel Frame Model Prototype

The design of the object consists of a steel frame structure with 5, 10, and 15 storeys using ST-37 (fy of 240 MPa steel) of 1 cm x 1 cm square dimension (Fig. 11). Steel base isolation support using spring parameter model, 1, 2, and 3 sliding rollers adopts a friction pendulum system with a curvature angle of 7º (Fig. 12).

Fig. 11 Three steel frame model prototype specimens for (a) 5 storeys; (b) 10 storeys; (c) 15 storeys

3.2. Steel Base Isolation

Steel base isolation support (using the spring parameter model) uses three different amounts of sliding rollers (1, 2, and 3 rollers) (Fig. 11). This support will be connected by bolts to existing steel support in the steel frame model.

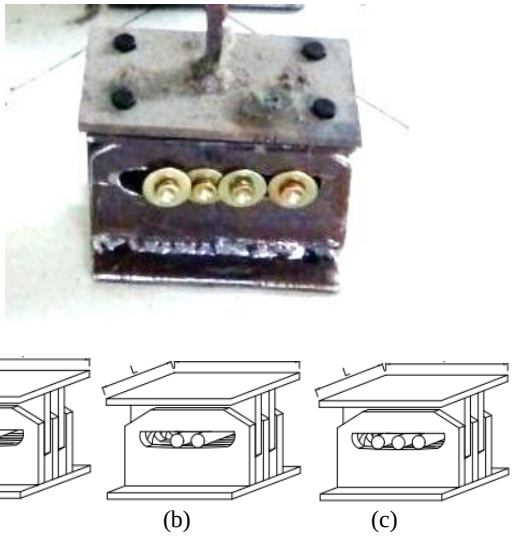

(a) (b) (c)

Fig. 12 Visualization of steel base isolator using (a) 1 roller; (b) 2 rollers; (c) 3 rollers

The testing setup scheme was illustrated in Fig. 13, and the shaking table setup was described in Fig. 14.

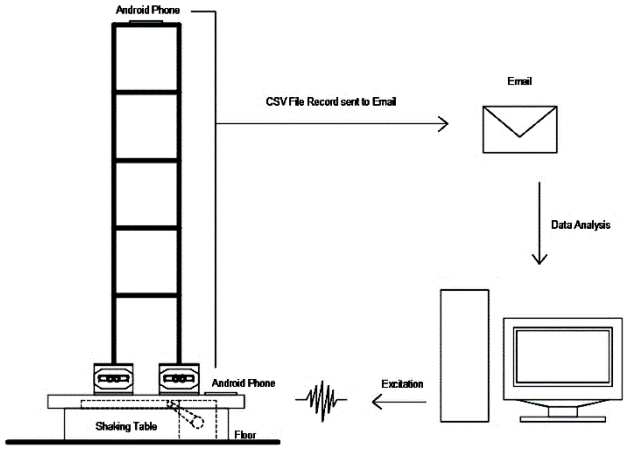

Fig. 13 Steel frame testing scheme using shaking table

Shaking table equipment is depicted in Fig. 14 with steel base isolation embedded in the support on the shaking table. Shaking direction is one direction shaking.

Fig. 14 The shaking table was attached to the base isolator supports through bolted connection

3.3. Dynamic Loads Input from Accelerometer

The following are the parameter of dynamic loads that will be inputted into the structures using time history data from the accelerometer.

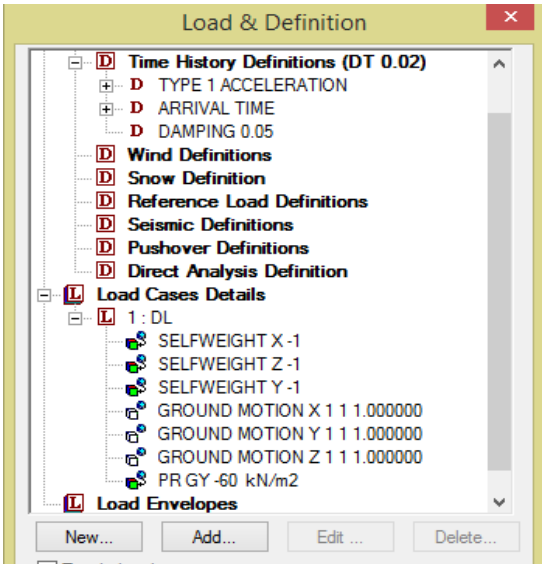

Fig. 15 Time history setting in STAAD Pro V8i

4. Results and Discussions

There are two kinds of analysis carried out: natural structural response analysis and dynamic analysis.

4.1. Natural Structural Response Analysis

The natural response of structures can be obtained by first inputting the geometry, the spring supports, and structure specification, then inputting the structural loads, including El Centro time history data into the software. From the analysis carried out, the natural frequency and mode shape on each frame were obtained as follows:

4.1.1. 5-Storey Steel Frame Model

From the calculation, obtained the frequency and natural period of the frame ($2\pi/\omega$) as follows:

ω_1 = 71,400 rad/dt T_1 = 0,088 detik
ω_2 = 118,551 rad/dt T_2 = 0,053 detik
ω_3 = 128,228 rad/dt T_3 = 0,049 detik
ω_4 = 241,661 rad/dt T_4 = 0,026 detik
ω_5 = 314,159 rad/dt T_5 = 0,020 detik

Based on the natural frequency values above, the mode shapes were obtained that represent each frequency (Fig. 16).

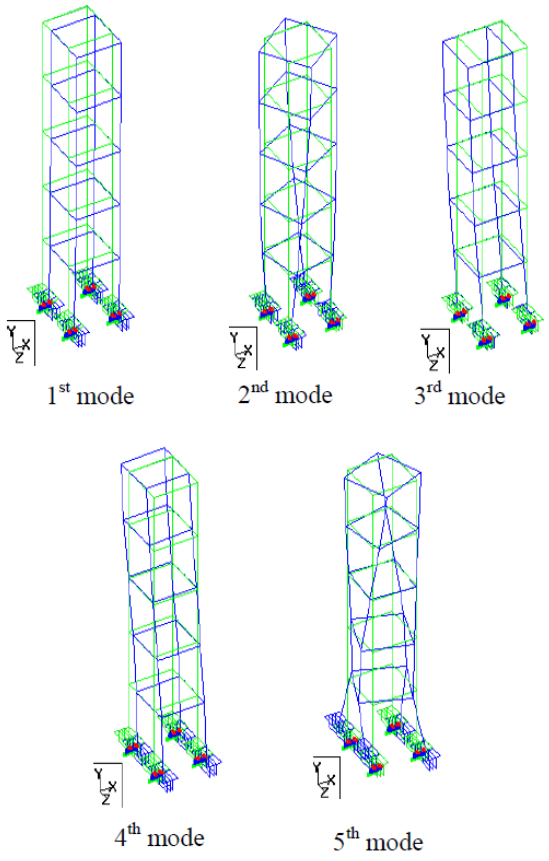

Fig. 16 Mode shapes on the 5-storey frame with roll support

Generally, the second mode was translation shape behavior, but the second mode occurred abnormally in a rotation shape because the four columns base is not fixedly supported, but they can slide depending on the shaking direction. However, for higher-level storeys (e.g., the 10th and 15th storeys), they behave normally as the second mode was the translational shape, and the third mode was the rotational shape (Fig. 17 and 18).

4.1.2. 10-Storey Steel Frame Model

From the analysis, obtained the frequency and natural period of the frame ($2\pi/\omega$) as follows:

ω_1 = 52,360 rad/s T_1 = 0,120 second
ω_2 = 62,832 rad/s T_2 = 0,100 second
ω_3 = 63,467 rad/s T_3 = 0,099 second
ω_4 = 142,800 rad/s T_4 = 0,044 second
ω_5 = 169,816 rad/s T_5 = 0,037 second
ω_6 = 190,400 rad/s T_6 = 0,033 second

Based on the natural frequency values above, the mode shapes were obtained that represent each frequency as follows:

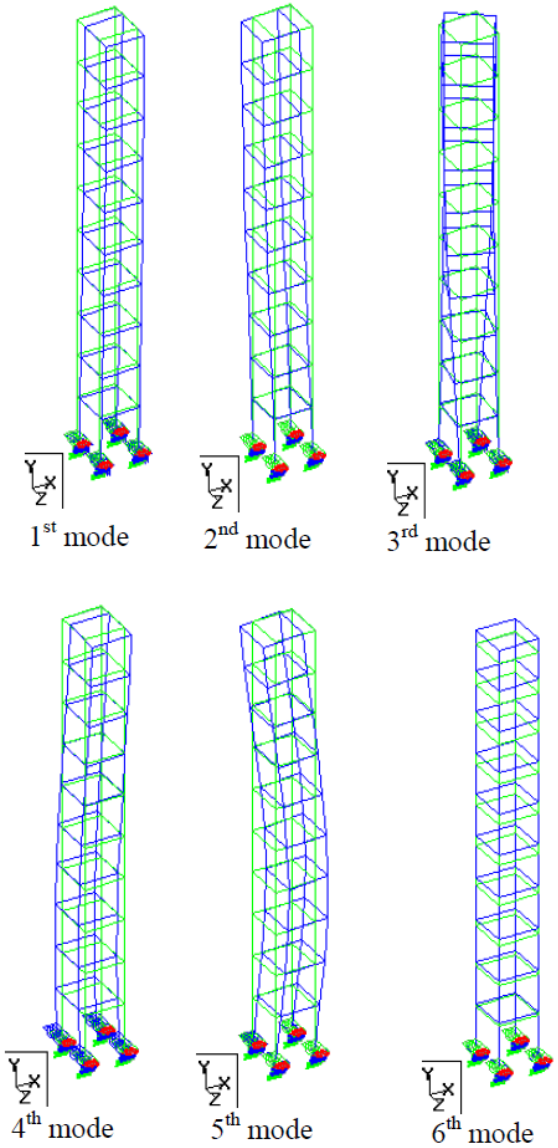

Fig. 17 Mode shape on 10-storey frame with roll support

4.1.3. 15-Storey Steel Frame Model

From the analysis, obtained the frequency and natural period of the frame ($2\pi/\omega$) as follows:

ω_1 = 36,319 rad/s T_1 = 0,173 second
ω_2 = 39,026 rad/s T_2 = 0,161 second

ω_3 = 43,036 rad/s T_3 = 0,146 second
ω_4 = 99,733 rad/s T_4 = 0,063 second
ω_5 = 112,200 rad/s T_5 = 0,056 second
ω_6 = 128,229 rad/s T_6 = 0,049 second

Based on the natural frequency values above, the mode shapes were obtained that represent each frequency as follows:

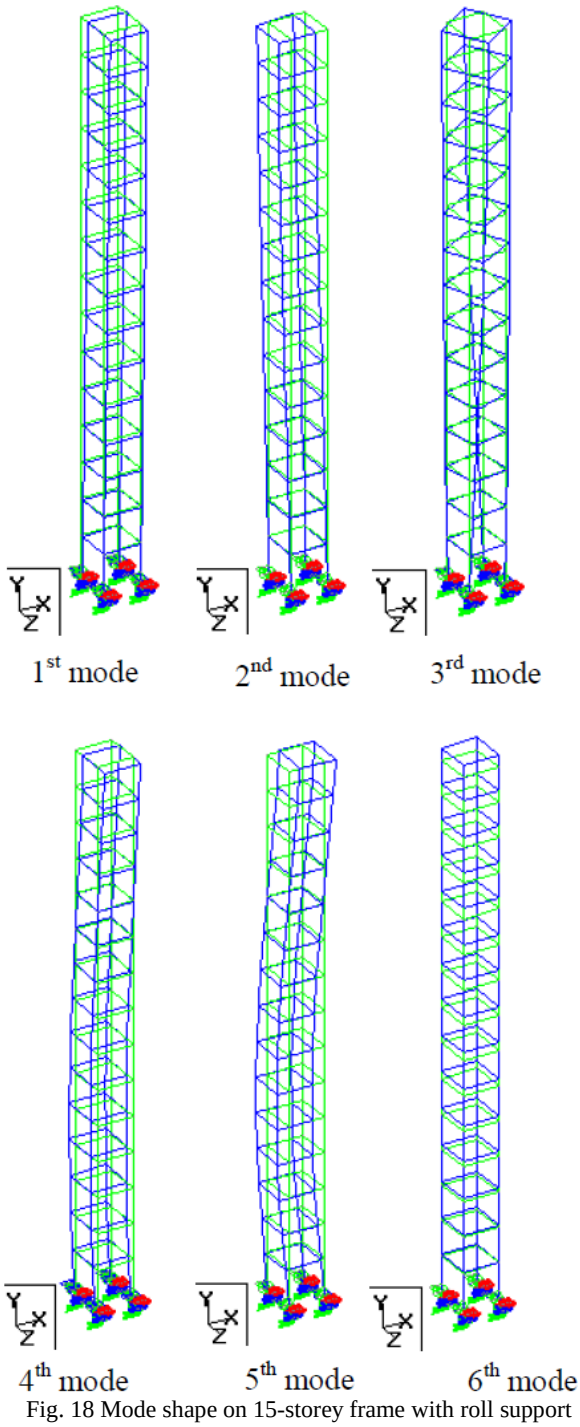

Fig. 18 Mode shape on 15-storey frame with roll support

4.2. Displacement Results

From the analysis results using El-Centro time history data, a table of the percentage ratio of displacement and acceleration on the frame roof was obtained.

Table *2* shows the roof displacement on each frame using base isolation with 1, 2, and 3 rollers. Fig. 19 also depicts the displacement results of each frame using base isolation for 1, 2, and 3 rollers. As described in Table 2, although the roller steel base isolation system was not effective enough for the 15-storey frame model for reducing the displacement, all rollers were the most effective base isolation for the 5-storey and 10-storey frame models using 3 rollers of this proposed steel base isolation type.

Table 2 Roof displacement ratio to 1 roller

Number of frame storeys	Number of rollers	Roof displacement (mm)	Ratio to 1 roller
5 storeys	1	1,05	100%
	2	0,53	50,93%
	3	0,38	36,42%
10 storeys	1	2,60	100%
	2	1,89	72,61%
	3	1,71	66,02%
15 storeys	1	6,72	100%
	2	6,57	97,79%
	3	6,48	96,47%

The displacement graph using all rollers is also depicted in Fig. 19 for 5, 10, and 15 storeys, clearly showing that 3 rollers give the best contribution to reducing displacement.

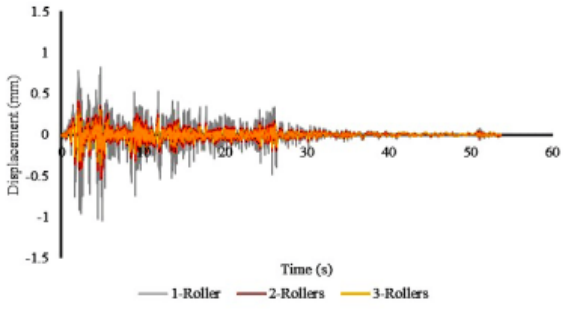

(a)

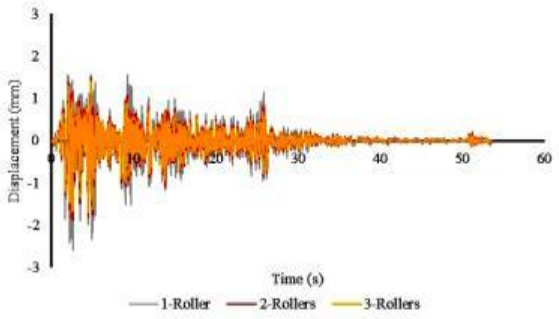

(b)

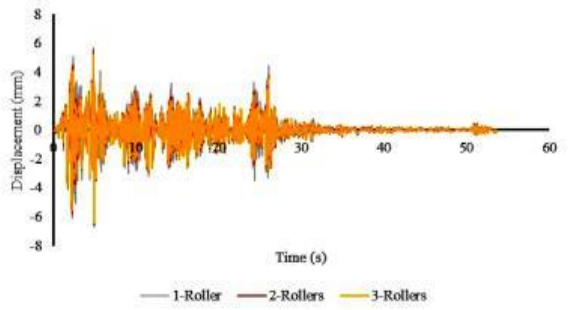

(c)

Fig. 19 Roof displacement of (a) 5-storey (b) 10-storey (c) 15-storey steel frame model using El-Centro

The 3-roller base isolation was suitable for the low level of the steel frame model. Ground floor displacement using the support of 1, 2, and 3 rollers is described in Fig. 20.

In Fig. 20, for a low-level steel frame such as the ground floor, the best displacement reduction was given by 3, 2, and 1 roller. But all the rollers fully contribute to reducing ground floor displacement.

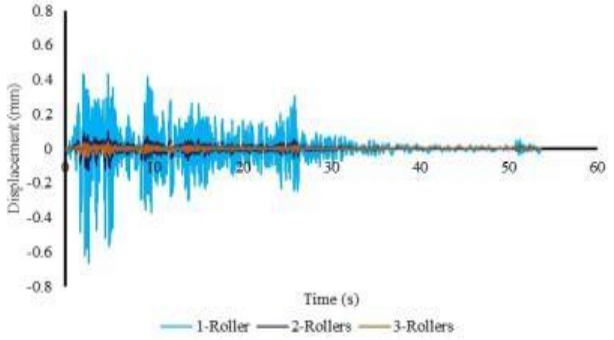

(a)

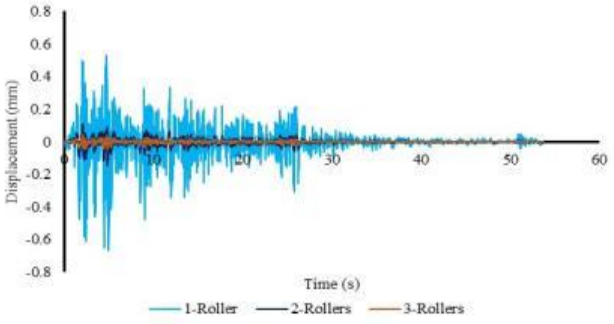

(b)

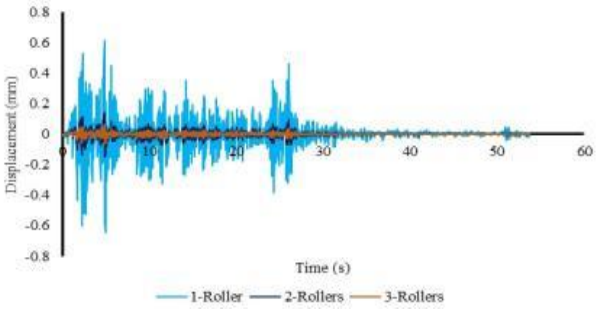

(c)

Fig. 20 Ground floor displacement of (a) 5-storey (b) 10-storey (c) 15-storey steel frame model

4.3. Acceleration Results

The comparison of the average roof acceleration on each frame using base isolation with 1, 2, and 3 rollers is described in Table 3. All roller types of the steel base isolation system are not effective enough for the 15-storey frame model for reducing the acceleration; all rollers, in fact, also give a non-significant reduction for the 5-storey and 10-storey frame models using this proposed steel base isolation type.

Table 3 Average roof acceleration ratio to 1 roller

Number of frame storeys	Number of rollers	Acceleration (m/s^2) Avg.	Ratio to 1 roller	Max.	Ratio to 1 roller
5 storeys	1	$2{,}2 .10^{-5}$	100%	2,46	100%
	2	$1{,}7 .10^{-5}$	79%	2,28	93%
	3	$2{,}0 .10^{-3}$	73%	1,70	69%
10 storeys	1	$3{,}2 .10^{-5}$	100%	4,47	100%
	2	$2{,}5 .10^{-5}$	78%	3,83	81%
	3	$2{,}5 .10^{-5}$	77%	3,53	74%
15 storeys	1	$8{,}7 .10^{-5}$	100%	7,79	100%
	2	$8{,}2 .10^{-5}$	94%	8,41	108%
	3	$7{,}7 .10^{-5}$	88%	8,37	108%

The maximum acceleration is depicted in Fig. 19 for 1, 2, and 3 rollers. But still, however the 3 rollers contribute most to reducing the acceleration.

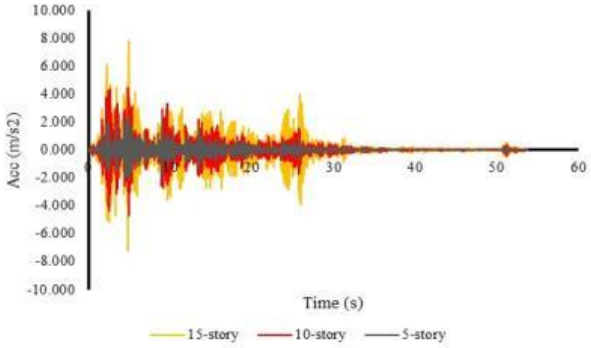

(a)

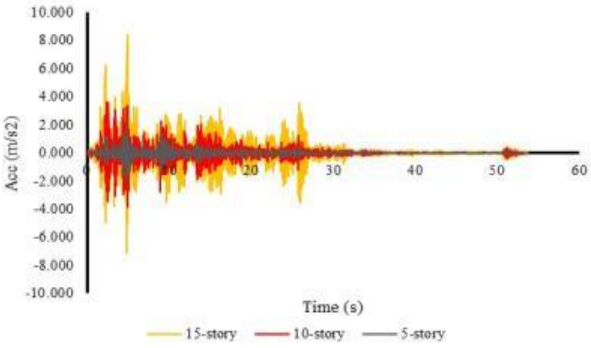

(b)

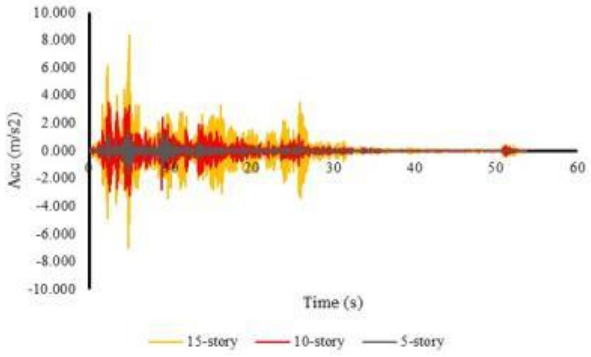

(c)

Fig. 21 Maximum roof acceleration on 5, 10, and 15 storeys: (a) 1 roller; (b) 2 rollers; (c) 3 rollers

4.4. Axial Force and Bending Moment Results

The comparison of axial force on 5-storey, 10-storey, and 15-storey steel frame models using base isolation with one, two, and three rollers are shown in Fig. 22.

In Fig. 24, amazingly, the axial force that occurred can be reduced for 5 and 10 storeys due to the transformation of seismic lateral force into the damped horizontal movement. However, in the 15 storeys, the reduction did not have too much impact because the

huge dead load was significantly increased, hence locking the roller from sliding movement.

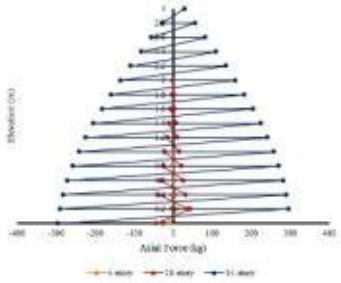

(a)

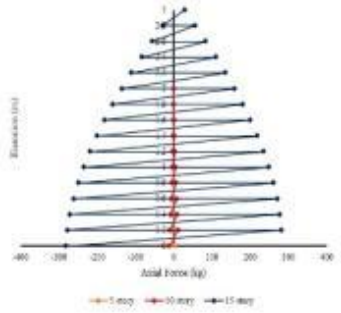

(b)

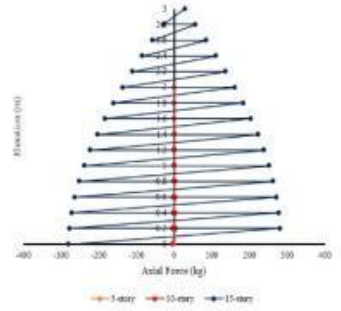

(c)

Fig. 22 Axial force in 5-, 10-, 15-storey steel frame using (a) 1 roller; (b) 2 rollers; (c) 3 rollers

The bending moment Y on 5-, 10-, and 15-storey steel frame models using base isolation with one, two, and three rollers is shown in Fig. 23.

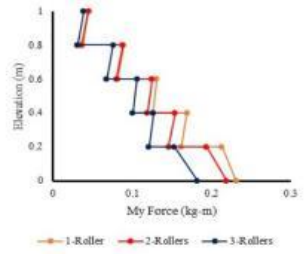

(a)

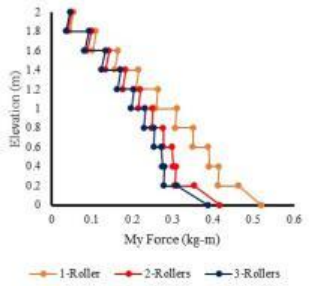

(b)

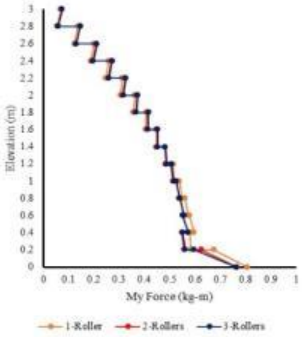

(c)

Fig. 23 The Bending Moment Y on (a) 5-storey frame; (b) 10-storey frame; (c) 15-storey frame

Fig. 23 shows that bending moment Y can be reduced in frames using base isolation best with 3, 2, and 1 roller, respectively. The bending moment Z on the 5, 10, and at the low level of 15-storey steel frame models using 1-, 2-, and 3-roller base isolation is shown in Fig. 24.

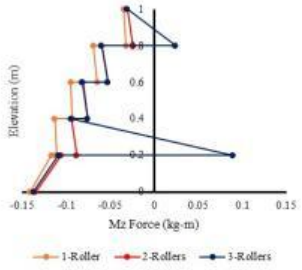

(a)

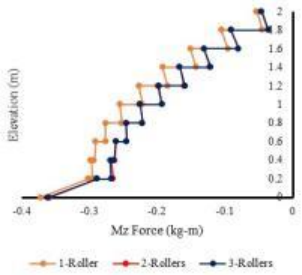

(b)

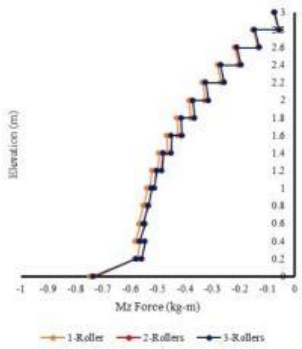

(c)

Fig. 24 The Bending Moment Z on (a) 5-storey frame; (b) 10-storey frame; (c) 15-storey frame

As shown in Fig. 24, it can be said that 2 and 3-rollers can be slightly reduced by bending moment Z value that occurred on 5 and 10 storeys, but not significant in 15-storey steel frames.

The inter-story drift values can be depicted in (c)

Fig. 25 on the 5, 10, and 15-storey frame model, which shows that the 3-roller support is effective only to reduce the drift ratio in low-level storeys, but at the roof, the values get close to one another.

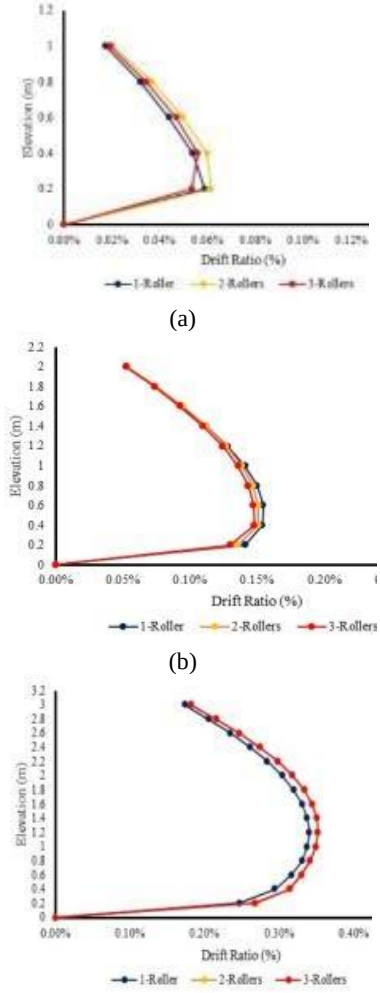

(a)

(b)

(c)

Fig. 25 Inter-story drift ratio of a) 5- b) 10- c) 15-storey steel frame using different amounts of sliding roller rods

The inter-story drift values can be depicted in (c)

Fig. 25 that occurs on the 10-storey and the 15-storey steel frame model and shows that the number of sliding rollers did not affect inter-story drift too much such as the ground floor inter-story drift ratio depicted by Fig. 26.

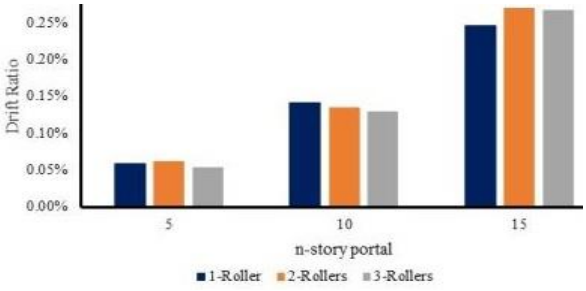

Fig. 26. The ground floor inter-story drift ratio

4.5. Shaking Table Dynamic Analysis

All three steel frame model structures' vibration test is carried out by using a shaking table. Similar to those in time history analysis, the acceleration ratio was found using 1, 2 and 3-rollers for shaking table and roof acceleration such as shown in Table 4 and 5.

Table 4 Shaking table acceleration ratio to 1 roller

Number of frame storeys	Number of rollers	Acceleration (m/s^2)			
		Avg.	Ratio to 1 roller	Max.	Ratio to 1 roller
5 storeys	1	0,17	100%	4.457	100%
	2	0,07	43%	4.156	93%
	3	0,03	20%	3.816	86%
10 storeys	1	0.04	100%	5.071	100%
	2	0.02	52%	4.280	84%
	3	0.03	58%	5.196	102%
15 storeys	1	0.04	100%	3.246	100%
	2	0.13	317%	4.756	147%
	3	0.12	278%	4.612	142%

The roof acceleration on each frame using 1, 2 and 3-rollers is in Table 5.

Table 5. Roof acceleration ratio to 1 roller

Number of frame storeys	Number of rollers	Acceleration (m/s^2)			
		Avg.	Ratio to 1 roller	Max.	Ratio to 1 roller
5 storeys	1	0,320	100%	5,848	100%
	2	0,259	81%	4,242	73%
	3	0,199	62%	3,802	65%
10 storeys	1	0,667	100%	6,220	100%
	2	0,531	80%	6,298	78%
	3	0,417	63%	6,314	101%
15 storeys	1	0,373	100%	6,314	100%
	2	0,407	109%	7,492	119%
	3	0,624	168%	7,136	113%

From the results obtained from Tables 4 and 5, it can be stated that all the rollers were suitable only for low levels such the 5th storey and one portion of 10 storeys by using 3 storeys indicate by lesser roof acceleration but getting higher at moderate to the high level of storeys such as the 10th (using 1 and 2 rollers) and 15th storeys.

The main cause of this behavior was in the moderate to high-level storeys (i.e., the 10th and 15th storeys) the dead load becomes significantly increased, hence it tends to lock the roller from sliding movement.

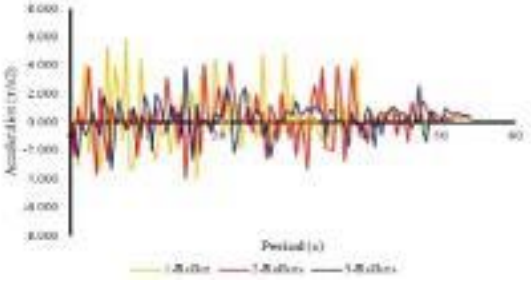

(a)

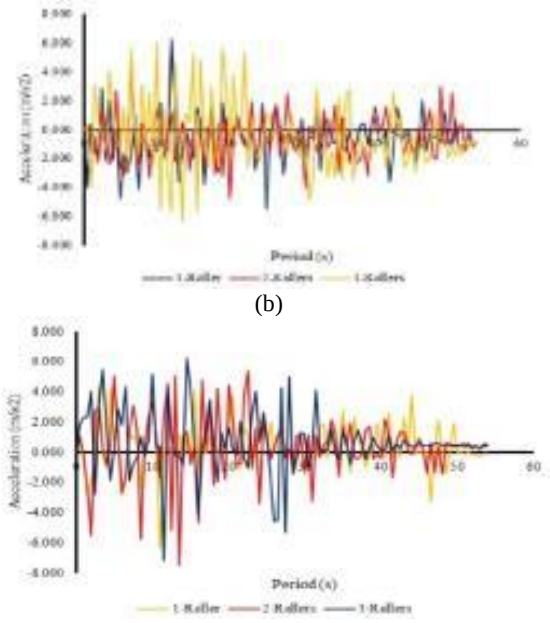

(b)

(c)

Fig. 27 Roof acceleration for (a) 5-storey; (b) 10-storey; (c) 15-storey steel frame models

The acceleration graph for steel frame models with respectively 5, 10, 15 storeys using different amounts of sliding roller rods was also depicted in Fig. 27.

In Fig. 27, the acceleration of 1 roller was too high compared to 2 and 3 rollers for all frame models. However, three rollers best contribute to reducing displacement and acceleration, especially this support type becomes the most effective in low-level storeys, such as the 5-storey frame model.

5. Conclusion

1) The obtained response ratio to withstand the model under El-Centro time history data:

a) Support with two rollers for the 10-storey frame having an average and maximum acceleration of 78% smaller and 81% smaller, respectively, and a maximum displacement of 73% smaller than those using 1-roller base isolation support.

b) Support with three rollers for the 5-storey frame model having an average and maximum acceleration of 73% and 69% smaller, respectively, and a maximum displacement of 36% smaller than those using 1-roller base isolation support.

2) The obtained response ratio to withstand the model under experimental shaking table test:

a. In moderate shaking vibration, support with two rollers for the 10-storey frame having an average and maximum acceleration of 48% smaller and 84% smaller than those using 1-roller base isolation support.

b. In moderate shaking vibration, support with three rollers for the 5-storey frame having an average and maximum acceleration of 62% smaller and 65% smaller than those using 1-roller base isolation support.

3) The optimum reduction was achieved by 3-roller sliding rods and likely tends to be better with a larger amount of sliding roller rods utilization with further research.

4) The optimum seismic responses reduction was significantly reduced by these new steel base isolation systems that only work with low-level steel frame models. The full-scale application is further needed considering the different returning curvatures for the appropriate amounts of the roller rods.

References

[1] WEKKE I. S., RAJINDRA R., PUSHPALAL D., SAMAD M. A., YANI A., and UMAM R. Educational Institution on Responding Disasters in Palu of Indonesia. Proceedings of the International Conference on Islam and Higher Education, Padang, 2019. https://osf.io/preprints/inarxiv/drc8q/download

[2] SUZUKI Y. Active fault and earthquake disasters. In: HIMIYAMA Y., SATAKE K., and OKI T. (eds.) *Human Geoscience. Advances in Geological Science*. Springer, Singapore, 2020: 99-117. https://doi.org/10.1007/978-981-32-9224-6_9

[3] WU J., HE X., LI Y., SHI P., YE T., and LI N. How earthquake-induced direct economic losses change with earthquake magnitude, asset value, residential building structural type and physical environment: An elasticity perspective. *Journal of Environmental Management*, 2019, 231: 321-328. https://doi.org/10.1016/j.jenvman.2018.10.050

[4] SUBRAMANI T., & SUJATHA S. Dynamic Analysis of Structure Subjected to Bi-Directional and Uni-Directional Earthquake Forces Using ETABS. *International Journal of Engineering & Technology*, 2018, 7(3.10): 108-114. https://doi.org/10.14419/ijet.v7i3.10.15641

[5] CHEN J., ZHAO C., XU Q., and YUAN C. Seismic analysis and evaluation of the base isolation system in AP1000 NI under SSE loading. *Nuclear Engineering and Design*, 2014, 278: 117-133. https://doi.org/10.1016/j.nucengdes.2014.07.030

[6] ZHOU F., & TAN P. Recent progress and application on seismic isolation energy dissipation and control for structures in China. *Earthquake Engineering and Engineering Vibration*, 2018, 17: 19–27. https://doi.org/10.1007/s11803-018-0422-4

[7] WICAKSONO A. D., & WAHYUNI E. Modifikasi Perencanaan Gedung RSUD Koja Jakarta Menggunakan Struktur Komposit Baja-Beton dengan Base Isolator: High Damping Rubber Bearing. *Jurnal Teknik ITS*, 2017, 6(2): D97-D102. https://doi.org/10.12962/j23373539.v6i2.24035

[8] KAMRAVA A. Seismic isolators and their types. *Current World Environment*, 2015, 10: 27-32. http://www.cwejournal.org/vol10noSpecial/seismic-isolators-and-their-types/

[9] FALBORSKI T., & JANKOWSKI R. Experimental Study on Effectiveness of a Prototype Seismic Isolation System Made of Polymeric Bearings. *Applied Sciences*, 2017, 7(8): 808. https://doi.org/10.3390/app7080808

[10] KUMAR M., WHITTAKER A. S., and CONSTANTINOU M. C. An advanced numerical model of elastomeric seismic isolation bearings. *Earthquake Engineering and Structural Dynamics*, 2014, 43: 1955–1974. https://doi.org/10.1002/eqe.2431

[11] KONSTANTINIDIS D., & NIKFAR F. Seismic response of sliding equipment and contents in base-isolated

buildings subjected to broadband ground motions. *Earthquake Engineering and Structural Dynamics*, 2015, 44: 865– 887. https://doi.org/10.1002/eqe.2490

[12] YU Y., ROYEL S., LI J., LI Y., and HA Q. Magnetorheological elastomer base isolator for earthquake response mitigation on building structures: modeling and second-order sliding mode control. *Earthquakes and Structures*, 2016, 11(6): 943-966. https://doi.org/10.12989/eas.2016.11.6.943

[13] MATICHARD F., LANTZ B., MITTLEMAN R., MASON K., KISSEL J., ABBOTT B., BISCANS S., MCIVER J., ABBOTT R., ABBOTT S., ALLWINE E., BARNUM S., BIRCH J., CELERIER C., CLARK D., COYNE D., DEBRA D., DEROSA R., EVANS M., FOLEY S., FRITSCHEL P., GIAIME J. A., GRAY C., GRABEEL G., HANSON J., HARDHAM C., HILLARD M., HUA W., KUCHARCZYK C., LANDRY M., LE ROUX A., LHUILLIER V., MACLEOD D., MACINNIS M., MITCHELL R., O'REILLY B., OTTAWAY D., PARIS H., PELE A., PUMA M., RADKINS H., RAMET C., ROBINSON M., RUET L., SARIN P., SHOEMAKER D., STEIN A., THOMAS J., VARGAS M., VENKATESWARA K., WARNER J., and WEN S. Seismic isolation of Advanced LIGO: Review of strategy, instrumentation and performance. *Classical and Quantum Gravity*, 2015, 32(18): 185003. https://doi.org/10.1088/0264-9381/32/18/185003

[14] HUANG J., SHI Z., HUANG W., CHEN X., and ZHANG Z. A periodic foundation with rotational oscillators for extremely low-frequency seismic isolation: analysis and experimental verification. *Smart Materials and Structures*, 2017, 26(3): 035061. http://dx.doi.org/10.1088/1361-665X/aa5dd1

[15] HABIEB A. B., MILANI G., and TAVIO T. Two-step advanced numerical approach for the design of low-cost unbonded fiber reinforced elastomeric seismic isolation systems in new masonry buildings. *Engineering Failure Analysis*, 2018, 90: 380-396. https://doi.org/10.1016/j.engfailanal.2018.04.002

[16] XU Z.-D., GAI P.-P., ZHAO H.-Y., HUANG X.-H., and LU L.-Y. Experimental and theoretical study on a building structure controlled by multi-dimensional earthquake isolation and mitigation devices. *Nonlinear Dynamics*, 2017, 89: 723–740. https://doi.org/10.1007/s11071-017-3482-5

[17] FAGÀ E., CERESA P., NASCIMBENE R., MORATTI M., and PAVESE A. Modelling curved surface sliding bearings with bilinear constitutive law: effects on the response of seismically isolated buildings. *Materials and Structures*, 2016, 49: 2179–2196. https://doi.org/10.1617/s11527-015-0642-2

[18] DI MATTEO A., FURTMÜLLER T., ADAM C., and PIRROTTA A. Optimal design of tuned liquid column dampers for seismic response control of base-isolated structures. *Acta Mechanica*, 2018, 229: 437–454. https://doi.org/10.1007/s00707-017-1980-7

[19] FU W., ZHANG C., SUN L., ASKARI M., SAMALI B., CHUNG K. L., and SHARAFI P. Experimental Investigation of a Base Isolation System Incorporating MR Dampers with the High-Order Single Step Control Algorithm. *Applied Sciences*, 2017, **7**(4): 344. https://doi.org/10.3390/app7040344

[20] BUDIONO B., & SETIAWAN A. Studi Komparasi Sistem Isolasi Dasar High-Damping Rubber Bearing dan Friction Pendulum System pada Bangunan Beton Bertulang. *Jurnal Teknik Sipil*, 2014, 21(3): 179-196. https://doi.org/10.5614/jts.2014.21.3.1

[21] CARDONE D., GESUALDI G., and BRANCATO P. Restoring capability of friction pendulum seismic isolation systems. *Bulletin of Earthquake Engineering*, 2015, 13: 2449–2480. https://doi.org/10.1007/s10518-014-9719-5

[22] CASTALDO P., & RIPANI M. Optimal design of friction pendulum system properties for isolated structures considering different soil conditions. *Soil Dynamics and Earthquake Engineering*, 2016, 90: 74-87. https://doi.org/10.1016/j.soildyn.2016.08.025

[23] RYAN K. L., & DAO N. D. Influence of vertical ground shaking on horizontal response of seismically isolated buildings with friction bearings. *Journal of Structural Engineering*, 2016, 142(1): 04015089. https://doi.org/10.1061/(ASCE)ST.1943-541X.0001352

[24] KRAVCHUK N., COLQUHOUN R., and PORBAHA A. *Development of a Friction Pendulum Bearing Base Isolation System for Earthquake Engineering Education*. Proceedings of the 2008 American Society for Engineering Education Pacific Southwest Annual Conference, 2008. https://engineering.purdue.edu/UCIST/publications/publications/Base%20isolation%20system_Ali.pdf

[25] WANG Y. P. Fundamentals of seismic base isolation. International Training Programs for Seismic Design of Building Structures, 2002. https://www.researchgate.net/publication/239556839_Fundamentals_of_Seismic_Base_Isolation

[26] KASIMZADE A. A., ŞAFAK E., VENTURA C. E., NAEIM F., and MUKAI Y. (eds.) *Seismic Isolation, Structural Health Monitoring, and Performance Based Seismic Design in Earthquake Engineering: Recent Developments*. Springer, Cham, 2019. https://doi.org/10.1007/978-3-319-93157-9

[27] HARVEY JR. P. S., & KELLY K. C. A review of rolling-type seismic isolation: Historical development and future directions. *Engineering Structures*, 2016, 125: 521-531. https://doi.org/10.1016/j.engstruct.2016.07.031

[28] ROCHMAN T., RASIDI N., SUMARDI S., and PURNOMO F. A new form of steel base isolation system for seismic high-rise building. *IOP Conference Series: Materials Science and Engineering*, 2020, 732(1): 012010. https://doi.org/10.1088/1757-899X/732/1/012010

[29] CANCELLARA D., & DE ANGELIS F. Dynamic assessment of base isolation systems for irregular in plan structures: Response spectrum analysis vs nonlinear analysis. *Composite Structures*, 2019, 215: 98-115. https://doi.org/10.1016/j.compstruct.2019.02.013

[30] ZHAI Z., GUO W., YU Z., HU Y., and MA C. Seismic performance assessment of steel strip dampers equipped in high-rise steel frame. *Journal of Constructional Steel Research*, 2021, 177: 106437. https://doi.org/10.1016/j.jcsr.2020.106437

[31] MAGUIRE J. R., TEH L. H., CLIFTON G. C., and MCCARTHY T. J. Equivalent static force method for selective storage racks with uplifting baseplates. *Journal of Constructional Steel Research*, 2020, 165: 105821. http://dx.doi.org/10.1016/j.jcsr.2019.105821

[32] SALIM M. A., & SISWANTO A. B. *Rekayasa Gempa*. K-Media, Yogyakarta, 2018.

[33] PAZ M., & KIM Y. H. *Structural Dynamics: Theory and Computation*. Springer, Cham, 2019.

https://doi.org/10.1007/978-3-319-94743-3
[34] DAZIO A. *Fundamentals of Structural Dynamics*. An-Najah National University, Nablus, 2013. https://www.academia.edu/37736958/Fundamentals_of_Structural_Dynamics_1_Course_description

参考文:

[1] WEKKE I. S.、RAJINDRA R.、PUSHPALAL D.、SAMAD M. A.、YANI A. 和 UMAM R. 印度尼西亚帕卢灾害应对教育机构。伊斯兰与高等教育国际会议论文集，巴东，2019。
https://osf.io/preprints/inarxiv/drc8q/download
[2] SUZUKI Y. 活动断层与地震灾害。见：HIMIYAMA Y.、SATAKE K. 和 OKI T. (编辑。) 人文地球科学。地质科学进展。新加坡施普林格，2020：99-117。
https://doi.org/10.1007/978-981-32-9224-6_9
[3] WU J., HE X., LI Y., SHI P., YE T., 和 LI N. 地震直接经济损失如何随地震震级、资产价值、住宅建筑结构类型和物理环境变化：弹性视角。环境管理杂志，2019，231：321-328。
https://doi.org/10.1016/j.jenvman.2018.10.050
[4] SUBRAMANI T., & SUJATHA S. 使用 ETABS 对承受双向和单向地震力的结构进行动态分析。国际工程技术杂志，2018，7(3.10)：108-114.
https://doi.org/10.14419/ijet.v7i3.10.15641
[5] CHEN J., ZHAO C., XU Q., 和 YUAN C. 美联社1000 NI基础隔震系统在上证所载荷下的地震分析与评价。核工程与设计，2014，278：117-133。
https://doi.org/10.1016/j.nucengdes.2014.07.030
[6] 周峰, 谭平. 中国结构隔震耗能与控制研究进展及应用. 地震工程与工程振动，2018，17：19-27。
https://doi.org/10.1007/s11803-018-0422-4
[7] WICAKSONO A. D., & WAHYUNI E. 使用钢-混凝土组合结构对雅加达古哈医院大楼的规划进行修改基础隔振器：高阻尼橡胶轴承。技术期刊它的，2017，6(2)：D97-D102。https://doi.org/10.12962/j23373539.v6i2.24035
[8] KAMRAVA A. 隔震器及其类型。当前世界环境，2015，10：27-32。
http://www.cwejournal.org/vol10noSpecial/seismic-isolators-and-their-types/
[9] FALBORSKI T., & JANKOWSKI R. 由聚合物轴承制成的原型隔震系统有效性的实验研究。应用科学，2017，7(8): 808. https://doi.org/10.3390/app7080808
[10] KUMAR M.、WHITTAKER A. S. 和 CONSTANTINOU M. C. 弹性隔震支座的高级数值模型。地震工程和结构动力学，2014，43：1955-1974。
https://doi.org/10.1002/eqe.2431
[11] KONSTANTINIDIS D., & NIKFAR F. 受宽带地面运动影响的基础隔离建筑物中滑动设备和内容物的地震响应。地震工程与结构动力学，2015，44：865–887。
https://doi.org/10.1002/eqe.2490
[12] YU Y., ROYEL S., LI J., LI Y., 和 HA Q. 用于建筑结构地震响应缓解的磁流变弹性体基础隔离器：建模和二阶滑模控制。地震与结构，2016，11(6)：943-966。
https://doi.org/10.12989/eas.2016.11.6.943
[13] MATICCHARD F., LANTZ B., MITTLEMAN R., MASON K., KISSEL J., ABBOTT B., BISCANS S., MCIVER J., ABBOTT R., ABBOTT S., ALLWINE E., BARNUM S. , BIRCH J., CELERIER C., CLARK D., COYNE D., DEBRA D., DEROSA R., EVANS M., FOLEY S., FRITSCHEL P., GIAIME JA, Grey C., GRABEEL G., HANSON J ., HARDHAM C., HILLARD M., HUA W., KUCHARCZYK C., LANDRY M., LE ROUX A., LHUILLIER V., MACLEOD D., MACINNIS M., MITCHELL R., O'REILLY B., 渥太华D., PARIS H., PELE A., PUMA M., RADKINS H., RAMET C., ROBINSON M., RUET L., SARIN P., SHOEMAKER D., STEIN A., THOMAS J., VARGAS M. 、VENKATESWARA K.、WARNER J. 和 WEN S. 高级LIGO的隔震：策略、仪器和性能回顾。经典和量子引力，2015，32（18）：185003。https://doi.org/10.1088/0264-9381/32/18/185003
[14] HUANG J., SHI Z., HUANG W., CHEN X., 和 ZHANG Z. 用于极低频隔震的带有旋转振荡器的周期性基础：分析和实验验证。智能材料与结构，2017，26(3)：035061.
http://dx.doi.org/10.1088/1361-665X/aa5dd1
[15] HABIEB A. B.、MILANI G. 和 TAVIO T. 在新砌体建筑中设计低成本非粘合纤维增强弹性隔震系统的两步高级数值方法。工程失效分析，2018，90：380-396。
https://doi.org/10.1016/j.engfailanal.2018.04.002
[16] XU Z.-D., GAI P.-P., ZHAO H.-Y., HUANG X.-H., 和 LU L.-Y. 多维隔震减振装置控制的建筑结构实验与理论研究.非线性动力学，2017，89：723-740。
https://doi.org/10.1007/s11071-017-3482-5
[17] FAGÀ E.、CERESA P.、NASCIMBENE R.、MORATTI M. 和 PAVESE A. 用双线性本构定律建模曲面滑动轴承：对隔震建筑物的响应的影响。材料与结构，2016，49：2179-2196。https://doi.org/10.1617/s11527-015-0642-2
[18] DI MATTEO A.、FURTMÜLLER T.、ADAM C. 和 PIRROTTA A. 用于基础隔震结构地震响应控制的调谐液柱阻尼器的优化设计。机械学报，2018，229：437-454。https://doi.org/10.1007/s00707-017-1980-7
[19] FU W.、ZHANG C.、SUN L.、ASKARI M.、SAMALI B.、CHUNG K. L. 和 SHARAFI P. 将先生阻尼器与高阶单步控制算法相结合的基础隔离系统的实验研究。应用科学，2017，7(4)：344.
https://doi.org/10.3390/app7040344
[20] BUDIONO B., & SETIAWAN A. 基本绝缘系统的比较研究高阻尼橡胶轴承担摩擦摆系统关于钢筋混凝土建筑。土木工程杂志，2014，21(3)：179-196。
https://doi.org/10.5614/jts.2014.21.3.1
[21] CARDONE D.、GESUALDI G. 和 BRANCATO P. 摩擦摆隔震系统的恢复能力。地震工程公报，2015，13：2449-2480。 https://doi.org/10.1007/s10518-014-9719-5
[22] CASTALDO P., & RIPANI M. 考虑不同土壤条件的孤立结构摩擦摆系统特性的优化设计。土壤动力学与地震工程，2016，90：74-87。
https://doi.org/10.1016/j.soildyn.2016.08.025
[23] RYAN K. L., & DAO N. D. 垂直地面震动对带有摩擦轴承的隔震建筑物水平响应的影响。结构工程杂志，2016，142(1)：04015089.
https://doi.org/10.1061/(ASCE)ST.1943-541X.0001352
[24] KRAVCHUK N.、COLQUHOUN R. 和 PORBAHA A.

开发用于地震工程教育的摩擦摆轴承底座隔振系统。2008年美国工程教育学会太平洋西南地区年会论文集，2008。https://engineering.purdue.edu/UCIST/publications/publications/Base%20isolation%20system_Ali.pdf
[25] WANG Y.P. 基础隔震基础。建筑结构抗震设计国际培训计划，2002. https://www.researchgate.net/publication/239556839_Fundamentals_of_Seismic_Base_Isolation
[26] KASIMZADE A. A.、ŞAFAK E.、VENTURA C. E.、NAEIM F. 和 MUKAI Y.（编辑）地震工程中的隔震、结构健康监测和基于性能的抗震设计：最新发展。斯普林格，湛, 2019. https://doi.org/10.1007/978-3-319-93157-9
[27] 小哈维。 P. S., & KELLY K. C. 滚动式隔震综述：历史发展和未来方向。工程结构，2016，125：521-531。https://doi.org/10.1016/j.engstruct.2016.07.031
[28] ROCHMAN T.、RASIDI N.、SUMARDI S. 和 PURNOMO F. 一种新型高层抗震钢基础隔震系统。眼压会议系列：材料科学与工程，2020，732(1): 012010. https://doi.org/10.1088/1757-899X/732/1/012010
[29] CANCELLARA D., & DE ANGELIS F. 不规则平面结构基础隔离系统的动态评估：响应谱分析与非线性分析。复合结构，2019，215：98-115。https://doi.org/10.1016/j.compstruct.2019.02.013
[30] ZHAI Z., GUO W., YU Z., HU Y., 和 MA C. 高层钢框架钢带阻尼器的抗震性能评估。建筑钢研究杂志，2021，177：106437。https://doi.org/10.1016/j.jcsr.2020.106437
[31] MAGUIRE J. R.、TEH L. H.、CLIFTON G. C. 和 MCCARTHY T. J. 具有提升底板的选择性存储架的等效静力方法。建筑钢研究杂志，2020，165：105821。http://dx.doi.org/10.1016/j.jcsr.2019.105821
[32] SALIM M. A. 和 SISWANTO A. B. 地震工程。韩媒，日惹，2018。
[33] PAZ M., & KIM Y. H. 结构动力学：理论与计算。斯普林格，湛， 2019. https://doi.org/10.1007/978-3-319-94743-3
[34] DAZIO A. 结构动力学基础。安纳杰国立大学，纳布卢斯，2013。https://www.academia.edu/37736958/Fundamentals_of_Structural_Dynamics_1_Course_description